Journal of Zhejiang University-SCIENCE A (Applied Physics & Engineering)
ISSN 1673-565X (Print); ISSN 1862-1775 (Online)
www.jzus.zju.edu.cn; www.springerlink.com
E-mail: jzus@zju.edu.cn

Numerical study on the dynamic response of a massive liquefied natural gas outer tank under impact loading*

Chen YAN[1,2], Xi-mei ZHAI[†‡1,2], Yong-hui WANG[1,2]

[1]*Key Lab of Structures Dynamic Behavior and Control of the Ministry of Education, Harbin Institute of Technology, Harbin 150090, China*

[2]*Key Lab of Smart Prevention and Mitigation of Civil Engineering Disasters of the Ministry of Industry and Information Technology, Harbin Institute of Technology, Harbin 150090, China*

[†]E-mail: xmzhai@hit.edu.cn

Received Apr. 29, 2019; Revision accepted Sept. 26, 2019; Crosschecked Oct. 10, 2019

Abstract: In this paper, the dynamic response of a typical 160 000 m^3 liquefied natural gas (LNG) prestressed concrete outer tank under impact loading is investigated. The applicability of the Holmquist-Johnson-Cook (HJC) material model of concrete and numerical simulation method on impact that is proposed in this paper is verified by the test results of concrete slabs under projectile impact cited from the reference. A detailed finite element (FE) model of the LNG outer tank, including walls, buttresses, domes, beams, and bottom plates, under the impact of a Tomahawk cruise missile is established. In addition, pre-stress on the wall, impact angles, locations, and velocities are considered and their influence on dynamic response studied. The impact damage types for the LNG outer tank are concluded according to dynamic response results including stress, displacement, stress sweep range, and energy, and critical impact velocities to distinguish these damage types are also determined. In addition, the damage types and their failure mechanism are analyzed by the damage factor proposed in this paper, which is based on energy propagation. Finally, four empirical formulas of impact loading recommended by the standard "accident analysis for aircraft crash into hazardous facilities" are used for checking the impact resistance performance of the LNG outer tank and compared with FE numerical simulation results. It is demonstrated, by using empirical formulas, that the common 160 000 m^3 LNG outer concrete tank could suffer flange impact loading. However, all the four empirical results were more conservative compared to numerical results under the same missile perforation velocity.

Key words: Liquefied natural gas (LNG) tank; Impact; Dynamic response; Numerical simulation; Failure mechanism
https://doi.org/10.1631/jzus.A1900172 **CLC number:** TU352

1 Introduction

Liquefied natural gas (LNG), generally stored in LNG tanks, is increasingly used as a major source of clean energy. Recently, exclusive studies on sloshing loads in LNG tanks (Lee et al., 2007; Graczyk and Moan, 2008) and the seismic performance of LNG tanks have been carried out (Christovasilis and Whittaker, 2008; Zhang et al., 2011). In addition, the influence of the liquefied natural gas itself, such as its temperature and pressure, on the LNG tank has also been analyzed (Chen et al., 2004). However, there are few studies on a LNG tank under impact loading. Since the LNG tank is massive in volume and complicated in structure, its mechanical performance under impact loading (such as conventional weapons) still needs to be studied. The impact may cause damage to the inner structure or structural failure. Furthermore, it will cause massive economic losses and secondary disasters such as fires and blasts due to the leaking of the cryogenic liquids in the tank.

‡ Corresponding author
* Project supported by the National Natural Science Foundation of China (No. 51978208)
ORCID: Chen YAN, https://orcid.org/0000-0002-6910-0320; Xi-mei ZHAI, https://orcid.org/0000-0002-3358-0481

Therefore, research on the impact resistance of extra-large LNG tanks is particularly important.

Research on LNG storage tanks has been carried out for more than 30 years and design codes have been issued, such as the Japanese design code (Dong and Zhang, 1996), the European design code (European Committee for Standardization, 2006), the British design code (British Standards Institution, 1993), and the American design code (American Petroleum Institute, 2008). When designing a tank under impact, the British design code assumes the flying object to be a rigid body weighing 50 kg with a velocity of 45 m/s.

Studies of a LNG tank under impact loading are few. The LNG tank is mainly fabricated from concrete and the impact is local. Hence, the response of a LNG tank under impact loading is similar to the behavior of concrete slabs or nuclear containment subjected to projectile impact, both of which have been extensively studied. Several methods, including experiments, numerical simulations, and empirical formulas, have been employed to obtain the dynamic responses of concrete slabs subjected to a projectile impact, such as the impact from a missile (Tai and Tang, 2006; Beppu et al., 2008; Forquin and Erzar, 2010; Rahman et al., 2010; Beckmann et al., 2011; Ranjan et al., 2014; Hu et al., 2017; Liu et al., 2018; Xu et al., 2019). All these experiments on the concrete slab showed four main processes: the spalling of the concrete, the scabbing of the concrete, projectile penetration into the target, and perforation of the target (Li et al., 2005). In terms of numerical simulation, ABAQUS was used to simulate aircraft impact on nuclear containers (Prabhakar et al., 2003; Daudeville and Malécot, 2011; Iqbal et al., 2012; Sadique et al., 2013) and concrete structures. LS-DYNA was used to simulate the aircraft impact on the World Trade Center (Karim and Fatt, 2005; Omika et al., 2005). All these studies indicate that using the finite element (FE) method to simulate impact on structures like the LNG tank is feasible. In order to obtain accurate results from the simulation, a suitable constitutive model is important. Several concrete constitutive models have been proposed for describing the mechanical behavior of concrete under impact loading (Johnson and Cook, 1983; Holmquist et al., 1993; Malvar et al., 1997; Murray, 2007). Experiments have also been carried out to evaluate the dynamic response of a concrete beam under drop-weight impact. They showed that concrete was stronger and absorbed more energy under impact loading compared with static loading (Adhikary et al., 2015; Rehacek et al., 2015). Zhang et al. (2017) investigated a model for aircraft engine impact on ultra-high performance steel fiber reinforced concrete (UHP-SFRC) panels and proposed a modified empirical formula for predicting the engine missile residual velocity. Zhang et al. (2018) modified the formula for a rigid projectile based on the present and existing test data to predict the penetration depth in reinforced concrete (RC) panels hit by a deformable engine. Although some suggestions have been given for impact resistance of LNG tanks, the failure types of external concrete tanks under impact loading and the influence of concrete grade, projectile mass, impact velocity, etc. on the response of an LNG outer tank still need to be studied. Hence, it is necessary to study the dynamic response of the LNG tank under impact loading.

In this paper, LS-DYNA is used to simulate the impact performance of a LNG tank based on the practical LNG tank project. The LNG outer tank's response characteristics under missile impact with different velocities, angles, and locations are studied. Rebars and prestressed rebars and their influences are also taken into consideration. The failure types of the structure under impact loading and the methods to identify these failure types are described. The failure mechanism for each failure type is analyzed. A damage factor for predicting which damage type will happen is given. Four empirical formulas are used to check whether in practice a 160 000 m^3 LNG tank can suffer the impact of flange and projectile suggested in the British design code. Numerical simulation results are compared with empirical ones. The findings from this study can provide the basis for impact resistance design of the LNG tank.

2 Introduction of the LNG project

A 160 000 m^3 LNG tank consists of two parts: the outer and inner tanks. The inner tank is built with 9% nickel steel. The outer tank, consisting of the wall and dome, is fabricated from prestressed concrete. The geometric parameters of the outer tank investigated in this study are given in Fig. 1. In this project, the concrete grade is C40 with cube compressive

strength of 40 MPa and the grade of rebar is HRB400 with yield strength of 400 MPa.

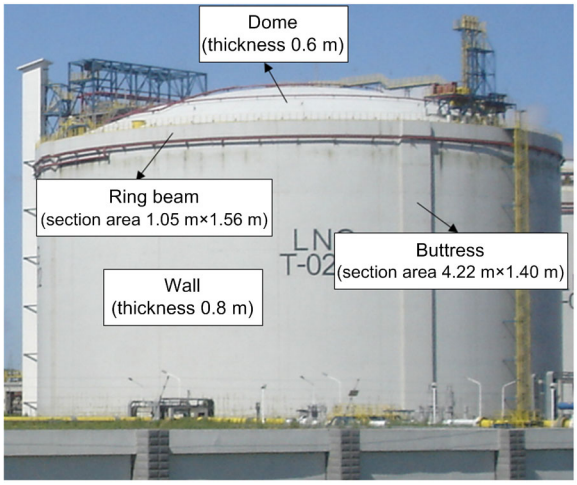

Fig. 1 LNG tank

3 FE model establishment

3.1 Element type and basic assumptions

Due to the complex geometry of the LNG tank and the complicated mechanical behavior of the tank under impact loading, it is necessary to select the appropriate element type when establishing the FE model. The eight-node brick element with reduced integration is employed for the wall and dome of the LNG tank as well as the impact projectile. The following assumptions about the impact projectile are made in this study to simplify the calculation: (1) the impact projectile is rigid and any deformation is ignored; (2) the heat loss during impact is not considered; (3) the friction between the impact projectile and the wall of the LNG tank wall is ignored during consideration of the impact process.

3.2 Concrete constitutive model

The choice of material constitutive relations will directly affect the calculation results. Hence, a suitable constitutive relation is an important prerequisite for the effective numerical simulation. Several constitutive models of concrete under high rate loading have been developed (Holmquist et al., 1993; Malvar et al., 1997). The Holmquist-Johnson-Cook (HJC) concrete model and continuous surface cap model (CSCM) are the most common concrete constitutive models. The CSCM concrete model (Murray, 2007) is easy to use but it is hard to control the yield surface when only inputting the unconfined compressive strength, mass density, and maximum aggregate size. To simulate the LNG tank under impact of a projectile, the HJC material model is used because it can predict the behavior of concrete under large strain, high strain rate, and high pressure. Its behavior has been verified in simulations of concrete structures under impact loading (Karim and Fatt, 2005; Tai and Tang, 2006; Rajput and Iqbal, 2017). Although tensile cracking in plain concrete targets cannot be predicted due to the limitations of the HJC model, it is adequate to model the fracture in the concrete under projectile impact because the compressive wave will reduce the tensile cracking (Rajput and Iqbal, 2017). The Saint Venant criterion that is based on the maximum principal strain is used in this study. Therefore, the HJC model is suitable for predicting the behavior of concrete and can be used in the present numerical simulation. The yield surface of the HJC model can be represented as

$$\sigma^* = \left[A(1-D)+BP^{*N}\right](1+C\ln\dot{\varepsilon}^*), \tag{1}$$

where $\sigma^*=\sigma/f_c'$ is defined as the normalized equivalent stress which is the ratio of actual equivalent stress to quasi-static uniaxial compressive strength, $P^*=p/f_c'$ is defined as the normalized hydrostatic pressure, A is the normalized cohesive strength, D is the material damage which ranges from 0 to 1, B is the normalized pressure hardening coefficient, N is the pressure hardening exponent, C is the strain rate coefficient, and $\dot{\varepsilon}^*=\dot{\varepsilon}/\dot{\varepsilon}_0$ is the normalized strain rate which is the ratio of the equivalent strain rate to the reference strain rate. The damage factor D can be expressed as

$$D=\sum\frac{\Delta\varepsilon_p+\Delta\mu_p}{\varepsilon_p^f+\mu_p^f}, \tag{2}$$

where $\Delta\varepsilon_p$ is the increment of the effective plastic strain, and $\Delta\mu_p$ is the increment of the plastic volumetric strain. $\varepsilon_p^f+\mu_p^f$ is the plastic strain to fracture and can be represented as

$$\varepsilon_{\mathrm{p}}^{\mathrm{f}}+\mu_{\mathrm{p}}^{\mathrm{f}}=D_1\left(P^*+T^*\right)^{D_2}, \tag{3}$$

where D_1 and D_2 are damage parameters. $T^*=T/f_c'$ is the normalized maximum tensile hydrostatic pressure, and T is the maximum tensile hydrostatic pressure. When $P^*=-T^*$, the concrete cannot withstand any plastic strain. According to the concrete strength grade (C40) in this study, the concrete constitutive model parameters can be set as: density is 2400 kg/m^3, the quasi-static uniaxial compressive strength is 48 MPa, and other parameters are default (Holmquist et al., 1993).

The ADD_EROSION option is used to simulate the failure of the concrete element. In this option, the maximum principal strain is defined as 0.1. It means that once the maximum principle strain of the element is larger than 0.1, the element is removed from the calculation. The contact type is erosion surface to surface (ESTS). In this contact type, although the failure element is deleted, the rest of the elements can still be considered in the calculation. The gain structure of material forming in the zone will change in the metal forming processes, such as stamping, deep drawing, bending, and punching. Grains are elongated or compressed along the direction of the processing, which is accompanied by hardening. Strength characteristics, such as yield strength, tensile strength, or hardness, will be enhanced because of the hardening effect. At the same time, toughness characteristics, such as elongation, constriction, and impact properties, are reduced. Geometric tolerance of precision parts can fluctuate significantly because of grain flow and intensity changes in the stamping process.

3.3 FE model verification with the impact experiments

In order to verify the applicability and accuracy of the established FE model in this study, the numerical results were compared with the experimental results of a concrete slab under projectile impact (Dong et al., 2005). Two circular concrete slabs with thicknesses of 80 mm and 150 mm were adopted; the diameter of both slabs is 1200 mm. A ballistic gun with a caliber of 35 mm was used as the launching device. The impact projectile was fabricated from high strength chromium molybdenum alloy. The shape of the projectile was a combined cylinder and hemisphere with a weight of 588–597 g, a diameter of 35 mm, and a length of 150 mm. The impact velocity and the residual velocity were collected by a velocity measuring device. The front and back sides of the 80-mm thick slab after impact are shown in Fig. 2. Following the geometry and material properties of the slabs (Dong et al., 2005), a FE model is established. The HJC model was used for the concrete slab and the eight-node brick element was adopted both for the projectile and the concrete slab. The mesh size is about 3.3 mm×3.3 mm×3.3 mm in the impact area. The ADD_EROSION option and ESTS contact type are used.

The whole process of the projectile impact on the slab is reproduced utilizing the FE simulation. Fig. 3 illustrates the perforation process in an 80 mm thick concrete slab subjected to a projectile impact with a velocity of 376 m/s.

Fig. 2 compares the front and back sides of the concrete slab from test and FE simulation, and a good agreement between the two can be observed in respect of spalls of concrete. From Table 1, it can be found that the error of residual velocity between FE simulation results and the experimental results of Dong et al. (2005) is less than 5%. This error can be accepted and it also provides the basis for the accuracy of the numerical simulation of the impact.

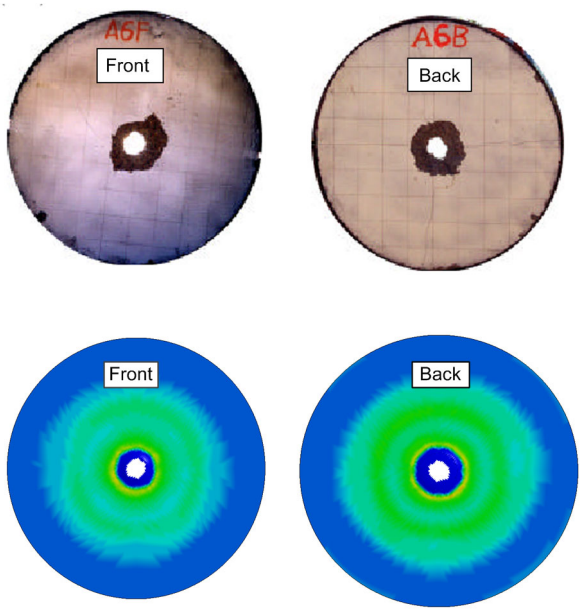

Fig. 2 Impact perforation (experimental and FE results)

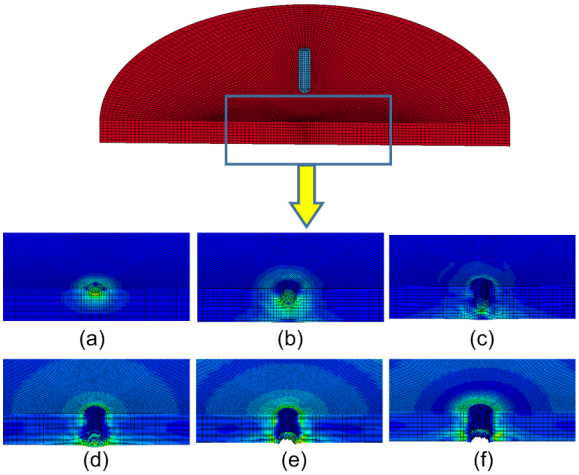

Fig. 3 Whole process of the impact perforation
(a) Time t=0.0003 s; (b) t=0.00037 s; (c) t=0.00045 s; (d) t=0.0005 s; (e) t=0.0006 s; (f) t=0.05 s

Table 1 Comparisons of FE simulation and experiment

Specimen No.	Impact velocity (m/s)	Residual velocity (m/s)		$\frac{v_s - v_t}{v_t}$
		Experiment value (v_t)	Simulation value (v_s)	
A1	218	166	161	−3.01%
A2	250	199	189	−5.03%
A3	376	280	270	−3.57%
A4	620	529	518	−2.08%
B1	317	80	83	3.75%
B2	501	301	286	−4.98%
B3	753	554	547	−1.26%

The concrete density is 2400 kg/m^3. Specimen type is plain

3.4 FE modelling of the LNG outer tank

In order to consider the effect of rebar and prestressed rebar ducts on the LNG tank, the method of converting wall thickness is used, and the preliminary research work (Yan et al., 2018; Zhai et al., 2019) has confirmed that the wall thickness difference is within 1.2%. In addition, based on the results of prestressed rebar distribution, tensioned stress, and prestress loss, Zhai et al. (2014) gave the FE result and method of calculating the effect of prestressing of the LNG tank against impact response. It turns out that the nodal displacement of the impact point can be reduced by 2.8%–19.7%, which means that the prestressed rebar can improve the impact resistant capacity of the LNG tank. However, the improvement is limited. Hence, the rebars, prestressed rebars, and prestressed rebar ducts were not considered in the FE analysis.

Since the FE model of a LNG tank is massive and the influence of impact is generally local, a finer mesh is adopted for the impact zone (the range is 5 m near the point of the impact) utilizing the method of local mesh encryption in order to ensure the accuracy of impact calculation, and the element size of the encryption area is 0.1 m×0.1 m×0.1 m, whereas a relatively coarse element size of 1.0 m×1.0 m×0.2 m is adopted for the area a certain distance away from the impact zone. In this situation, the amount of computation is reduced and the reliability of the local impact can also be guaranteed. All nodes from the bottom plate are restricted from three translational degrees. Fig. 4 gives the 1/4 FE model of LNG outer tank that shows the different parts of the actual outer tank.

A Tomahawk cruise missile, as one of the conventional weapons, is selected as the impact projectile in this study. The weight is 1440 kg, the length is 6.25 m, the diameter of the head is 0.52 m, and the max velocity is 244 m/s. Different warhead shapes may bring different results and therefore the selection of the warhead shape is important. In this study, the warhead of the Tomahawk, which is close to hemispherical in shape, is simplified as a hemisphere. The missile is divided into five parts along the radial direction and ten parts along the length direction. The eight-node brick element is also adopted for the missile.

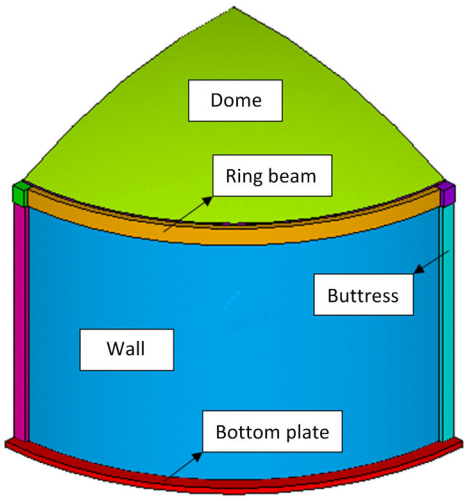

Fig. 4 1/4 FE model of the LNG outer tank

4 Dynamic responses of LNG outer tank under impact loading

4.1 Impact response of the dome

The center point of the dome was impacted by the missile model with mass of 1440 kg, velocity of 50 m/s, and diameter of 0.52 m. Since the impact duration is very short and the stress and strain of the LNG tank approach stability after 0.2 s, the whole impact calculation time is chosen to be 0.2 s. Fig. 5 is the von Mises stress of the LNG tank, which shows that the stress gradually spreads from the impact point to the nearby area and that the maximum stress was 78.34 MPa at the impact point. Due to the high strain rate and confinement effect of the concrete under impact, its ultimate strength under impact is larger than that under quasi-static uniaxial compression. As for the dome, six elements along the diagonal are selected which are marked as Q1–Q6 and the FE data are extracted. The location of each element is shown in Fig. 5.

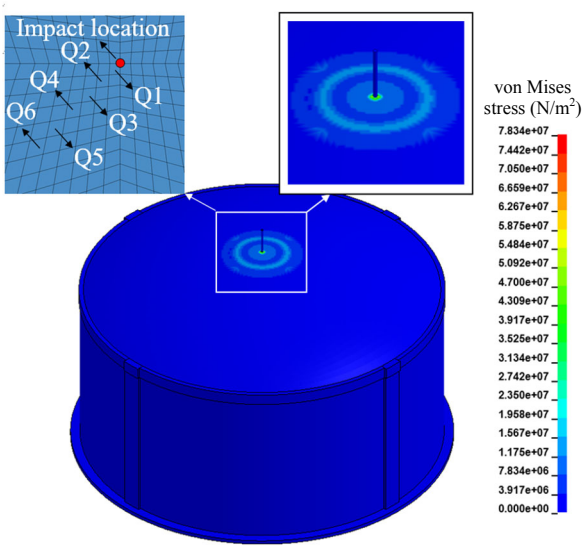

Fig. 5 von Mises stress of the LNG tank and element assignment of the LNG tank

The vertical displacement–time curve and von Mises stress–time curve of each element are shown in Figs. 6a and 6b, respectively. It is observed that the impact point of the dome deforms first and the nearby area deforms immediately after the deformation of the impact point. Then, the deformation range spreads out. At the same time, the impact point reaches its maximum stress. When the projectile impacts the dome, it passes its kinetic energy to the dome and the impact area accepts the energy immediately. Meanwhile, the stress and displacement reach their peak values. The stress then spreads out and gradually weakens. In addition, in order to understand the influence range of the impact, this study gives the quantitative description. The stress sweep range is defined as the maximum distance of the element stress of more than 50 MPa from the impact point. According to the above definition, the stress sweep range of this condition is 0.583 m, which shows that the impact is a local effect.

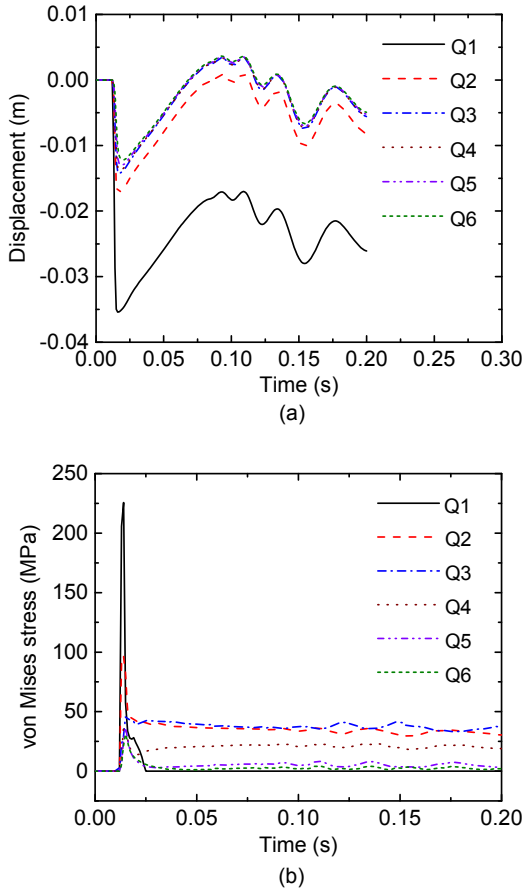

Fig. 6 Displacement–time curve (a) and von Mises stress–time curve (b) of elements on the dome

4.2 Parametric study of impact response

In this study, 30 impact cases are calculated by changing the impact location (wall top, middle, and bottom and buttress top, middle, and bottom), impact

velocity (40 m/s, 50 m/s, and 60 m/s), and impact angle (0°, 30°, and 60°). In the impact case WT-40-0 for example, W means wall, T means top, 40 means the impact velocity is 40 m/s, and 0 means the impact angle is 0°. Top, middle, and bottom mean the impact heights are 35 m, 17 m, and 2 m from the bottom plate, respectively.

4.2.1 Impact velocity

With different impact velocities, the impact angle remains 0° here. The maximum von Mises stress of the element measures the LNG outer tank's ability to withstand the impact force; the maximum displacement of the node reflects its ability to resist deformation, and the stress sweep range reflects the impact range. Hence, this study extracts, for each impact position, the maximum von Mises stress of the element, maximum displacement, and stress sweep range. It can be observed from Fig. 7a that a higher impact velocity with higher initial kinetic energy leads to higher maximum von Mises stress of the element. When the projectile impacts the outer tank with a higher velocity, the outer tank will receive more energy, and it will cause higher stress.

Table 2 shows the maximum displacement of the node and stress sweep range at different velocities. Increasing impact velocity results in higher maximum displacement of the node. When the projectile impacts the outer tank with a higher velocity, the outer tank receives more kinetic energy from the projectile which leads to its larger deformation. In addition, increasing the impact velocity also leads to an increase in the stress sweep range. This can also be explained by the increased kinetic energy received by the outer tank from the projectile.

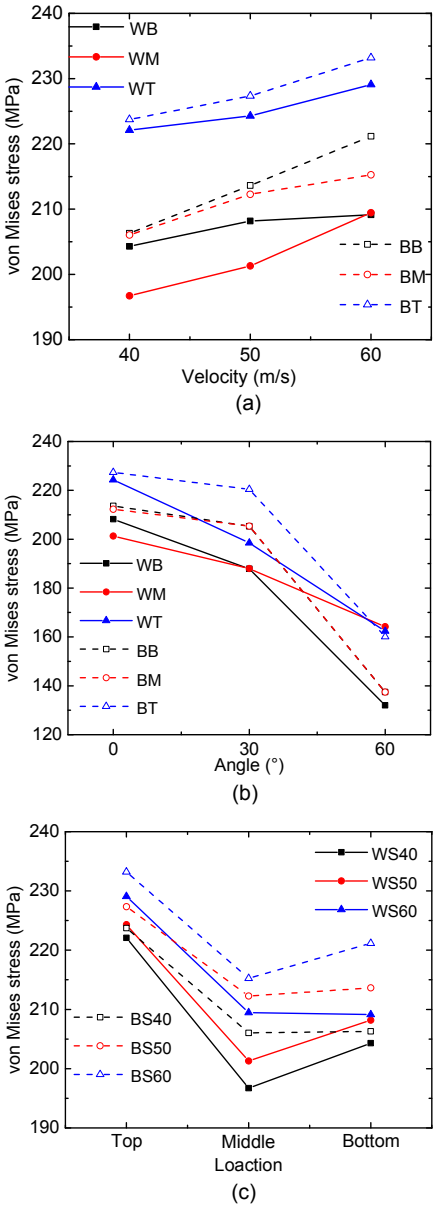

Fig. 7 Curves of elements on the wall: (a) stress–velocity curve; (b) stress–angle curve; (c) stress–location curve

Table 2 Displacement and stress sweep range under different impact velocities and angles

Velocity (m/s)	Angle (°)	WB		WM		WT		BB		BM		BT	
		MD (m)	SR (m)	MD (m)	SR (m)	MD (m)	SR (m)	MD (m)	SR (m)	MD (m)	SR (m)	MD (m)	SR (m)
40	0	0.054	0.367	0.054	0.393	0.052	0.361	0.046	0.400	0.050	0.424	0.047	0.392
50	0	0.066	0.500	0.066	0.583	0.065	0.500	0.058	0.566	0.062	0.566	0.059	0.533
60	0	0.080	0.640	0.080	0.640	0.078	0.640	0.069	0.603	0.073	0.640	0.070	0.603
50	0	0.066	0.500	0.066	0.583	0.065	0.500	0.058	0.566	0.062	0.566	0.059	0.533
50	30	0.041	0.424	0.041	0.500	0.042	0.424	0.043	0.500	0.041	0.495	0.038	0.500
50	60	0.016	0.283	0.016	0.361	0.016	0.283	0.018	0.300	0.013	0.241	0.017	0.241

MD means maximum displacement of the nodal, and SR means stress sweep range

4.2.2 Impact angle

With different impact angles, the impact velocity remains 50 m/s. The impact angle is defined as the angle between the center line of the missile and the missile projection line in the horizontal plane, including 0°, 30°, and 60°, and the vertical impact is 0°.

The maximum von Mises stress of the element, maximum displacement, and stress sweep range are extracted. The results are shown in Fig. 7b and Table 2. It is observed from Fig. 7b that a larger impact angle leads to a lower maximum von Mises stress of the element and less damage. The most unfavorable impact angle is 0°. The reason is that, when the impact angle is not 0°, the impact velocity can be decomposed into two directions, i.e. 0° and 90°, and the damage of the tank wall is mainly caused by the impact energy from the component of 0°. When the impact angle is larger, the component of 0° is smaller. Hence, the kinetic energy that the outer tank receives from the projectile is less, which leads to a lower maximum von Mises stress of the element. The effect of impact angle on the buttress also shows the same rule, i.e. a larger impact angle leads to lower maximum von Mises stress of the element of the buttress.

As can be seen from Table 2, an increasing impact angle leads to a decrease in maximum displacement. Similarly, the kinetic energy that the outer tank can receive from the projectile is less with a greater impact angle, which causes a smaller deformation. When the impact angle is less, the ability to resist deformation is worse. In addition, increasing the impact angle also leads to a decrease in stress range and impact area. Due to the lower stress under a larger impact angle, the impact area shows a decrease.

4.2.3 Impact location

The maximum von Mises stress of the element, maximum displacement, and stress sweep range are extracted. The results are shown in Fig. 7c and Table 2. As can be seen from Fig. 7c, the top part of the tank wall is most vulnerable, followed by the bottom part and finally the middle part. This is because the top part of the wall is connected to the ring beam which has greater stiffness and the stress therefore increases. The bottom part of the wall is connected to the bottom plate which also has greater stiffness. However, because the thickness of the ring beam is greater than that of the bottom plate, the stiffness of the top part is higher than that of the bottom part. The stiffness of the middle part is not changed. Similarly, the buttress has the same rule, as shown in Fig. 7c. At the same time, comparing the two values between the wall and the buttress, we can conclude that the stress of the buttress is higher than the wall, which can be attributed to the greater thickness of the buttress as compared to the wall.

It can be seen from Table 2 that the difference of maximum displacements of the nodes at different locations is very small. Hence, the maximum von Mises stress of the element with relatively more significant difference is used to determine the vulnerable position. Table 2 indicates that the maximum displacement of the node of the buttress is larger than that of the wall. This is the same as the maximum von Mises stress of the element. It can be seen from Table 2 that, at the same impact velocity, there is little difference of the stress sweep range in each location, which shows that the size of the impact area is not strongly related to the impact location.

4.3 Classification of impact damage of LNG outer tank

With the increasing of impact velocity, the failure of the concrete spreads from a single element to the surroundings. In addition, the perforation depth of the missile also increases with the increase of impact velocity. The failure magnitude of the concrete is closely related to the impact velocity of the missile, i.e. the higher the missile's velocity, the more serious the failure of the concrete. By changing the velocity of the impact projectile, the types of damage of the LNG outer tank are summarized in Table 3.

When the missile impacts the dome and its velocity is less than 75 m/s, the dome shows local distortion. When the velocity reaches 75 m/s, the concrete of the dome begins to spall. When the missile's velocity reaches 127 m/s, the missile penetrates the dome. In terms of the damage types of the wall under missile impact, the wall shows local distortion when the impact velocity is less than 66 m/s. When the velocity reaches 66 m/s, the concrete of the wall begins to spall. When the velocity of the missile reaches 147 m/s, the missile penetrates the wall. Based on the above observations, two critical velocities can be defined to separate these three damage types, i.e. the

first critical velocity for the beginning of the concrete spalling and the second critical velocity for the perforation of the LNG outer tank. Fig. 8 shows the von Mises stress of the dome with different damage types at time 0.02 s. The stress sweep range is also considered, as shown in Fig. 9.

Table 3 Damage classification under Tomahawk cruise and KongDi-63 missile

Damage type	Velocity for dome under TC (m/s)	Velocity for wall under TC (m/s)	Velocity for dome under KD (m/s)
Local distortion	0–75	0–66	0–78
Concrete spalling	75–127	66–147	78–111
Perforation	≥127	≥147	≥111

TC means Tomahawk cruise missile; KD means KongDi-63 missile

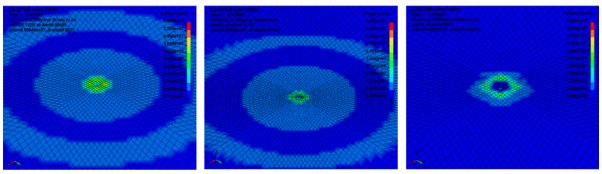

Fig. 8 von Mises stress of the impact area on the dome under different impact velocities: (a) v=50 m/s; (b) v=90 m/s; (c) v=130 m/s

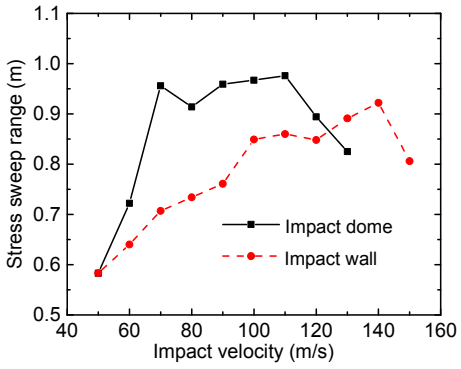

Fig. 9 Stress sweep range–impact velocity curves

Three kinds of impact velocity correspond to the three failure types. It can be seen from Fig. 8 that when the concrete has local distortion or fails, the stress propagation is evident. This is mainly because the ratio of energy absorbed by the failure of concrete is small when the velocity is not very high. Thus, the energy received from the projectile can be spread out. When perforation happens, a lot of energy is absorbed by the failing concrete which causes weaker stress propagation. This phenomenon can also be seen in Fig. 9, which shows that the stress propagation increases before the perforation and decreases after the perforation. Indeed, there is almost no stress propagation after the perforation. Meanwhile, as shown in Fig. 9, when the concrete of the dome has distortion, the stress sweep range mutates but this mutation is not significant when the missile impacts the wall.

At the same time, we also selected the KongDi-63 missile as an impact projectile. Table 3 shows the damage types. The first and second critical velocities are 78 and 111 m/s, respectively. Comparing the two kinds of critical velocities of the missiles reveals that their maximums are close. In this case, when the missile's diameter is larger, the first critical velocity increases and the second critical velocity decreases. In the impact resistant design of the LNG tank, more attention should be given to those impact projectiles that have small diameters and large masses. In this study, two kinds of missile are chosen as the impact projectiles and three damage types are identified, i.e. local distortion, concrete spalling, and perforation.

4.4 Failure mechanism of LNG outer tank

Failure mechanism of the LNG outer tank is given according to the different characteristics of internal energy during the whole impact process. The main reason for the three damage types is the initial impact energy. When the impact force is small, the initial energy is small and it will cause only local distortion. However, as the impact force is increased, the initial energy will increase too and damage such as concrete spalling and perforation will occur at that time. The whole impact process can be divided into three stages, i.e. energy application, energy transfer, and energy consumption. In the following sections, three examples will be used to explain the failure mechanisms of the three damage types.

4.4.1 Failure mechanism of local distortion

By using the example of the local distortion damage type (Tomahawk cruise missile impacts the dome with impact velocity v=50 m/s, as shown in Fig. 10), the failure mechanism is analyzed below.

The energy applying stage refers to the process at the impact of the missile on the dome. In this stage, the missile impacts the dome and it will transfer

kinetic energy to the dome. The impact zone receives the energy and then transfers it to internal energy, so the impact zone will have local distortion. The energy transfer stage means that the energy will transfer from the impact zone to the non-impact zone. In this stage, the energy is spreading out from the middle part and the missile is leaving the impact zone. The impact force is decreasing from 3.85×10^4 kN to 0 kN. The internal energy reaches the maximum value (1.1×10^6 J) and then decreases, as shown in Fig. 11. The energy consumption stage means that the missile is no longer contacting the dome. In this stage, the elements will vibrate and finally stop, so the internal energy will tend to stability. The internal energy finally reaches the stable value of 7.85×10^5 J.

4.4.2 Failure mechanism of concrete spalling

Failure mechanism is analyzed in the following section by using the example of the concrete spalling damage type (Tomahawk cruise missile impacts the dome with v=90 m/s, as shown in Fig. 10). Eroded internal energy means the energy of the deleted elements, residual internal energy means the residual energy of LNG tank after the impact, and total internal energy means the sum of eroded internal energy and residual internal energy. The energy applying stage shows no difference compared to the damage type of local distortion. However, as the speed of the missile is increased, its kinetic energy will increase, too. Thus, the total internal energy is larger: 3.3×10^6 J in this case. In the energy transfer stage, when the missile impacts the dome, some elements of the dome will fail and be deleted in the later calculation. The impact force decreases from 4.44×10^4 kN to 0 kN. The deleted elements consume the partial energy, which is the eroded internal energy (1.38×10^6 J), as shown in Fig. 11. The energy will still transfer from the impact zone to the non-impact zone. The residual internal energy reaches a maximum (1.92×10^6 J) and then decreases to 1.46×10^6 J. In the energy consumption stage, the residual elements will vibrate and finally stop, so the total internal energy will tend to stability, at 2.84×10^6 J.

4.4.3 Failure mechanism of perforation

By using the example of the perforation damage type (Tomahawk cruise missile impacts the dome with v=130 m/s, as shown in Fig. 10), failure mechanism is analyzed. In the energy applying stage, the missile impacts the dome and it will penetrate the dome immediately. The impact force reaches a peak of 4.67×10^4 kN and the total energy reaches the maximum (5.64×10^6 J), as shown in Fig. 11. The energy transfer stage shows that by deleting the failed concrete elements, most of the internal energy will be absorbed and the eroded internal energy increases to its peak (4.63×10^6 J). The residual internal energy first increases to the maximum (2.39×10^6 J) and then decreases to 6.50×10^5 J. It means that the energy will no longer transfer from the impact zone to the non-impact zone. The missile will penetrate the dome and enter the inside of the LNG tank. In the energy consumption stage, the residual elements will vibrate and finally stop, so the total internal energy will tend to stability at 5.28×10^6 J.

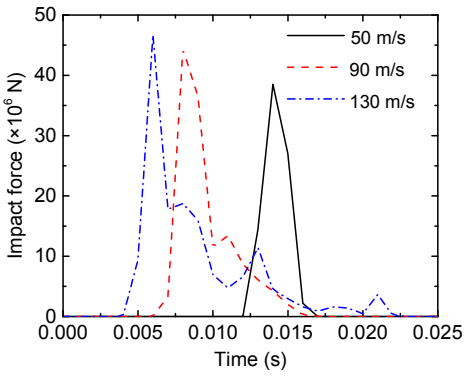

Fig. 10 Impact force–time curve

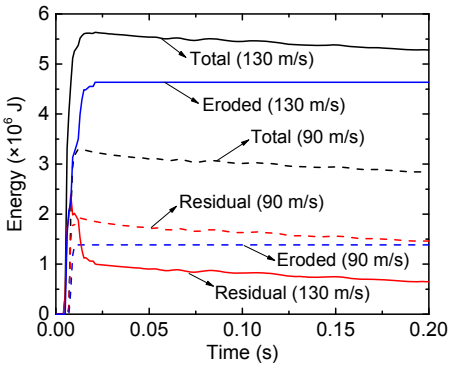

Fig. 11 Energy–time curve

4.5 Damage factor of LNG outer tank

Combining Sections 4.3 and 4.4, a parameter is given to predict which damage type will occur. The

parameter is defined as the damage factor (D_f). The equation for calculating the damage factor is

$$D_f=\frac{E_e}{E_t}, \tag{4}$$

where E_e is the maximum eroded internal energy and E_t the maximum total internal energy. E_e and E_t can be calculated through a numerical simulation, the curve between D_f and E_e can be seen in Fig. 12.

When D_f=0, there is no eroded internal energy. In this situation, the damage type will be local distortion. When $0<D_f\leq 0.8$, the damage type will be concrete spalling. When $D_f>0.8$, the damage type will be perforation.

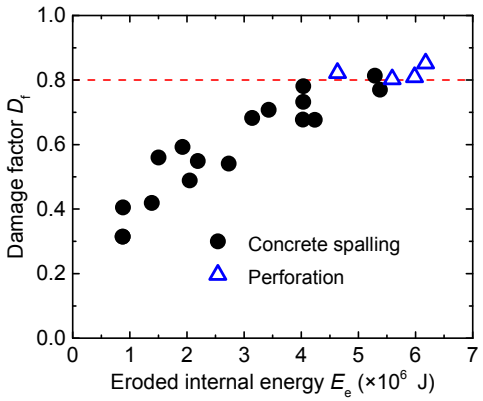

Fig. 12 Damage factor distribution

5 Empirical formulas

This paper selects four empirical formulas according to the standard "accident analysis for aircraft crash into hazardous facilities" (U.S. Department of Energy, 2006) which is proposed by the U.S. Department of Energy. According to these four formulas, two impacts are checked if the LNG outer tank can suffer the impact loading. Meanwhile, the results of numerical analysis are compared with the empirical formulas.

5.1 Introduction of empirical formulas

For checking the LNG outer tank under impact loading and simulating the minimum thickness of the outer tank, four empirical formulas are given in the Department of Energy standard (DOE-standard), as shown in Table 4. The formulas can be divided into two kinds, i.e. to prevent the concrete from scabbing, and perforation. For the wall, the scabbing thickness and perforation thickness should be checked. For the dome, only the perforation thickness should be checked.

5.2 Using the British standard for impact checking

For the impact loading, it is pointed out in the British standard BS7777-4 (British Standards Institution, 1993) that an impact object with a mass of 50 kg and a velocity of 45 m/s is reasonable. Table 5 gives the calculation results of the scabbing thickness (t_s) and perforation thickness (t_p) under the four formulas. The Tomahawk cruise missile with a diameter of 0.52 m is adopted as the impact object. The concrete grade is C40. According to the formula $f_c'=0.8f_c$, f_c' is 32 MPa (f_c is the cubic compressive strength, f_c' is the cylindrical compressive strength). The density is 2400 kg/m^3. From the calculation results, the most unfavorable scabbing thickness is 0.2496 m and the most unfavorable perforation thickness is 0.0842 m. To prevent scabbing, the minimum concrete thickness should be no less than $1.1t_s$, which is 0.275 m herein. To prevent perforation, the minimum concrete thickness should be no less than $1.2t_p$, which is 0.101 m herein. When the thickness of the LNG outer tank wall is 0.8 m and the dome thickness is 0.6 m, the tank can accept an impact such as that described in the British standard.

5.3 Using the flange for impact checking

Li et al. (2013) used the flange as the impact projectile for impact checking. The flange's effective diameter is 0.3 m, the mass is 110 kg, and the velocity is 45 m/s. Table 5 gives the calculation results of the scabbing and perforation thicknesses under the four formulas. The same concrete grade (C40) is also used. From the calculation results, the most unfavorable scabbing thickness is 0.3819 m and the most unfavorable perforation thickness is 0.1643 m. To prevent scabbing, the minimum concrete thickness should be no less than $1.1t_s$, which is 0.420 m. To prevent perforation, the minimum concrete thickness should be no less than $1.2t_p$, which is 0.197 m. The thickness of the LNG outer tank wall is 0.8 m and the dome thickness is 0.6 m, and therefore the tank can accept the flange as the impact projectile.

Table 4 Empirical formulas

Formula	Scabbing thickness, t_s	Perforation thickness, t_p
DOE-standard	$t_s = 1.84\left(\frac{U}{V}\right)^{0.13} \frac{(MV^2)^{0.4}}{D^{0.2}(f_c')^{0.4}}$	$t_p = \left(\frac{U}{V}\right)^{0.25}\left(\frac{MV^2}{Df_c'}\right)^{0.5}$
CEA-EDF	–	$t_p = 0.82(f_c')^{-0.375}\rho^{-0.125}\left(\frac{M}{D}\right)^{0.5} V^{0.75}$
Bechtel	$t_s = \frac{38.62}{\sqrt{f_c'}}\left(\frac{M^{0.4}V^{0.5}}{D^{0.2}}\right)$	–
CRIEPI	$t_s = 1.75\left(\frac{V_0}{V}\right)^{0.13} \frac{(MV^2)^{0.4}}{D^{0.2}(f_c')^{0.4}}$	$t_p = 0.90\left(\frac{V_0}{V}\right)^{0.25}\left(\frac{MV^2}{Df_c'}\right)^{0.5}$

U is the reference velocity given in the DOE-standard whose value is 60.96 m/s; V_0 is the reference velocity given in the CRIEPI whose value is 60.96 m/s; V is the impact velocity (m/s); M is the mass (kg); concrete density ρ is 2400 kg/m^3

5.4 Comparison of empirical and numerical results

From the numerical results, three conditions are obtained, i.e. the perforation velocities of a Tomahawk cruise missile impacting the dome and wall as well as the perforation velocity of a KongDi-63 missile impacting the dome. The numerical results of t_p (t_{pn}) can be calculated by the thickness of the practical project. The thicknesses of the wall and dome are 0.8 m and 0.6 m, respectively. But the thickness should be divided by a coefficient (1.2). According to the diameter and the mass of the projectile, the empirical results of t_p (t_{pe}) can be obtained and are given in Table 6.

It is observed that t_{pe} is larger than t_{pn} no matter which formula is used. It means that using empirical formulas to calculate the perforation thickness is safer than numerical results. It is also noted that the DOE-standard formula is the safest.

Table 5 Calculation results using British standard and flange

Formula	t_s (m)		t_p (m)	
	British standard	Flange	British standard	Flange
DOE-standard	0.22	0.33	0.08	0.16
CEA-EDF	–	–	0.08	0.16
Bechtel	0.25	0.38	–	–
CRIEPI	0.21	0.32	0.08	0.15

V=45 m/s; f_c'=32 MPa. For British standard, M=50 kg and D=0.52 m. For Flange, M=110 kg and D=0.3 m

Table 6 Comparisons of the empirical and numerical results

Impact case	Perforation velocity (m/s)	Numerical result, t_{pn} (m)	Empirical result, t_{pe} (m)		
			DOE-standard	CEA-EDF	CRIEPI
TC for dome	127	0.500	0.983	0.946	0.885
TC for wall	147	0.667	1.097	1.056	0.988
KD for dome	111	0.500	0.867	0.834	0.780

The diameter and the mass of the Tomahawk cruise missile (TC) are 0.52 m and 1440 kg, respectively. The diameter and the mass of the KongDi-63 missile (KD) are 0.76 m and 2000 kg, respectively. f_c' is 32 MPa

6 Conclusions

LS-DYNA was used to simulate the LNG outer tank under impact loading. The effect of rebar and prestressed rebar was very small. Parametric studies showed that both increasing impact velocity and reducing impact angle could lead to lower stress of the LNG outer tank and a larger impact range. The most unfavorable impact angle is 0°. The size of the impact range is not strongly related to the impact location. The most unfavorable impact location is the top part of the wall, followed by the bottom part of the wall, especially the connection between the wall and the ring beam and the connection between the wall and the bottom plate. These connections are the weakest points in the LNG outer tank and therefore more attention should be paid to them in impact resistant design.

Numerical simulation results showed that the LNG outer tank had three damage types, i.e. local distortion, concrete spalling, and perforation. The

critical velocities to distinguish these three damage types were also defined. The first and second critical velocities relate to the beginning of concrete spalling and the perforation of the LNG outer tank, respectively. The first critical velocity of a Tomahawk cruise missile impacting the dome (wall) is 75 m/s (66 m/s) and the second critical velocity is 127 m/s (147 m/s). The first critical velocity of KongDi-63 missile impacting the dome is 78 m/s and the second critical velocity is 111 m/s. The failure mechanism showed that the whole impact can be divided into three stages, i.e. energy application, energy transfer, and energy consumption. Different damage types showed different characteristics of impact force and energy changes. For the general situation, a method to predict which damage type will happen is to use the damage factor (D_f). When D_f=0, the damage type will be local distortion. When $0<D_f\leq 0.8$, the damage type will be concrete spalling. When $D_f>0.8$, the damage type will be perforation.

By using empirical formulas, the tank could accept the impact suggested by the British standard and the flange cited from the reference. Comparing numerical results with empirical results revealed that empirical results are conservative under the same projectile perforation velocity. From the three formulas, DOE-standard formula provided the most conservative prediction.

Contributors

Chen YAN and Xi-mei ZHAI designed the research and processed the corresponding data. Chen YAN wrote the first draft of the manuscript. Yong-hui WANG helped organize the manuscript. Chen YAN and Xi-mei ZHAI revised and edited the final version.

Conflict of interest

Chen YAN, Xi-mei ZHAI, and Yong-hui WANG declare that they have no conflict of interest.

References

Adhikary SD, Li B, Fujikake K, 2015. Low velocity impact response of reinforced concrete beams: experimental and numerical investigation. *International Journal of Protective Structures*, 6(1):81-111. https://doi.org/10.1260/2041-4196.6.1.81

American Petroleum Institute, 2008. Design and Construction of Large, Welded, Low-pressure Storage Tanks, API STANDARD 620. American Petroleum Institute, Washington, USA.

Beckmann B, Hummeltenberg A, Weber T, et al., 2011. Concrete under high strain rates: local material and global structure response to impact loading. *International Journal of Protective Structures*, 2(3):283-293. https://doi.org/10.1260/2041-4196.2.3.283

Beppu M, Miwa K, Itoh M, et al., 2008. Damage evaluation of concrete plates by high-velocity impact. *International Journal of Impact Engineering*, 35(12):1419-1426. https://doi.org/10.1016/j.ijimpeng.2008.07.021

British Standards Institution, 1993. Flat-bottomed, Vertical, Cylindrical Storage Tanks for Low Temperature Service, BS7777-4:1993. British Standards Institution, London, UK.

Chen QS, Wegrzyn J, Prasad V, 2004. Analysis of temperature and pressure changes in liquefied natural gas (LNG) cryogenic tanks. *Cryogenics*, 44(10):701-709. https://doi.org/10.1016/j.cryogenics.2004.03.020

Christovasilis IP, Whittaker AS, 2008. Seismic analysis of conventional and isolated LNG tanks using mechanical analogs. *Earthquake Spectra*, 24(3):599-616. https://doi.org/10.1193/1.2945293

Daudeville L, Malécot Y, 2011. Concrete structures under impact. *European Journal of Environmental and Civil Engineering*, 15(S1):101-140. https://doi.org/10.1080/19648189.2011.9695306

Dong J, Deng GQ, Yang KZ, et al., 2005. Damage effect of thin concrete slabs subjected to projectile impact. *Chinese Journal of Rock Mechanics and Engineering*, 24(4): 713-720 (in Chinese). https://doi.org/10.3321/j.issn:1000-6915.2005.04.029

Dong LS, Zhang SM, 1996. Design of LPG and LNG tanks in Japan. *Oil & Gas Storage and Transportation*, 15(5):51-53 (in Chinese).

European Committee for Standardization, 2006. Design and Manufacture of Site Built, Vertical, Cylindrical, Flat-bottomed Steel Tanks for the Storage of Refrigerated, Liquefied Gases with Operating Temperatures Between 0 °C and −165 °C, Part 1: General, EN 14620-1:2006. European Committee for Standardization, Brussels, Belgium.

Forquin P, Erzar B, 2010. Dynamic fragmentation process in concrete under impact and spalling tests. *International Journal of Fracture*, 163(1-2):193-215. https://doi.org/10.1007/s10704-009-9419-3

Graczyk M, Moan T, 2008. A probabilistic assessment of design sloshing pressure time histories in LNG tanks. *Ocean Engineering*, 35(8-9):834-855. https://doi.org/10.1016/j.oceaneng.2008.01.020

Holmquist TJ, Johnson GR, Cook WH, 1993. A computational constitutive model for concrete subjected to large strains, high strain rates, and high pressures. Proceedings of the 14th International Symposium on Ballistics, p.591-600.

Hu F, Wu H, Fang Q, et al., 2017. Impact performance of explosively formed projectile (EFP) into concrete targets. *International Journal of Impact Engineering*, 109:150-166.

https://doi.org/10.1016/j.ijimpeng.2017.06.010

Iqbal MA, Rai S, Sadique MR, et al., 2012. Numerical simulation of aircraft crash on nuclear containment structure. *Nuclear Engineering and Design*, 243:321-335. https://doi.org/10.1016/j.nucengdes.2011.11.019

Johnson GR, Cook WH, 1983. A constitutive model and data for metals subjected to large strains, high strain rates and high temperatures. Proceedings of the 7th International Symposium on Ballistics, p.541-547.

Karim MR, Fatt MS, 2005. Impact of the Boeing 767 aircraft into the world trade center. *Journal of Engineering Mechanics*, 131(10):1066-1072. https://doi.org/10.1061/(asce)0733-9399(2005)131:10(1066)

Lee DH, Kim MH, Kwon SH, et al., 2007. A parametric sensitivity study on LNG tank sloshing loads by numerical simulations. *Ocean Engineering*, 34(1):3-9. https://doi.org/10.1016/j.oceaneng.2006.03.014

Li JG, Zheng JH, Li H, et al., 2013. Verifying calculations of local effect of flying object impact on concrete outer tank of full containment LNG storage tank. *Petroleum Engineering Construction*, 39(4):30-33 (in Chinese). https://doi.org/10.3969/j.issn.1001-2206.2013.04.008

Li QM, Reid SR, Wen HM, et al., 2005. Local impact effects of hard missiles on concrete targets. *International Journal of Impact Engineering*, 32(1-4):224-284. https://doi.org/10.1016/j.ijimpeng.2005.04.005

Liu J, Wu CQ, Su Y, et al., 2018. Experimental and numerical studies of ultra-high performance concrete targets against high-velocity projectile impacts. *Engineering Structures*, 173:166-179. https://doi.org/10.1016/j.engstruct.2018.06.098

Malvar LJ, Crawford JE, Wesevich JW, et al., 1997. A plasticity concrete material model for DYNA3D. *International Journal of Impact Engineering*, 19(9-10):847-873. https://doi.org/10.1016/S0734-743X(97)00023-7

Murray YD, 2007. Users Manual for LS-DYNA Concrete Material Model 159. FHWA-HRT-05-062, Federal Highway Administration, McLean, USA.

Omika Y, Fukuzawa E, Koshika N, et al., 2005. Structural responses of world trade center under aircraft attacks. *Journal of Structural Engineering*, 131(1):6-15. https://doi.org/10.1061/(asce)0733-9445(2005)131:1(6)

Prabhakar G, Ranjan R, Mini KP, et al., 2003. Analysis of aircraft impact on containment structure. Proceedings of the 5th Asia-Pacific Conference on Shock & Impact Loads on Structures, p.315-322.

Rahman IA, Zaidi AMA, Bux Q, et al., 2010. Review on empirical studies of local impact effects of hard missile on concrete structures. *International Journal of Sustainable Construction Engineering and Technology*, 1(1):73-98.

Rajput A, Iqbal MA, 2017. Impact behavior of plain, reinforced and prestressed concrete targets. *Materials & Design*, 114:459-474. https://doi.org/10.1016/j.matdes.2016.10.073

Ranjan R, Banerjee S, Singh RK, et al., 2014. Local impact effects on concrete target due to missile: an empirical and numerical approach. *Annals of Nuclear Energy*, 68:262-275. https://doi.org/10.1016/j.anucene.2014.01.015

Rehacek S, Hunka P, Citek D, et al., 2015. Impact testing of concrete using a drop-weight impact machine. *Advanced Materials Research*, 1106:225-228. https://doi.org/10.4028/www.scientific.net/amr.1106.225

Sadique MR, Iqbal MA, Bhargava P, 2013. Nuclear containment structure subjected to commercial and fighter aircraft crash. *Nuclear Engineering and Design*, 260:30-46. https://doi.org/10.1016/j.nucengdes.2013.03.009

Tai YS, Tang CC, 2006. Numerical simulation: the dynamic behavior of reinforced concrete plates under normal impact. *Theoretical and Applied Fracture Mechanics*, 45(2):117-127. https://doi.org/10.1016/j.tafmec.2006.02.007

U.S. Department of Energy, 2006. Accident Analysis for Aircraft Crash into Hazardous Facilities, DOE-STD-3014-2006. U.S. Department of Energy, Washington, USA.

Xu XZ, Ma TB, Ning JG, 2019. Failure mechanism of reinforced concrete subjected to projectile impact loading. *Engineering Failure Analysis*, 96:468-483. https://doi.org/10.1016/j.engfailanal.2018.11.006

Yan C, Zhai XM, Wang YH, 2018. Numerical simulation of a large LNG concrete outer tank under impact loads. *Journal of Harbin Engineering University*, 39(9):1517-1525 (in Chinese). https://doi.org/10.11990/jheu.201703059

Zhai XM, Gao S, Fan F, 2014. Mechanical behavioral of LNG outer concrete tank under low temperature. *Journal of Harbin Institute of Technology*, 46(4):7-12 (in Chinese). https://doi.org/10.11918/j.issn.0367-6234.2014.04.002

Zhai XM, Zhao XY, Wang YH, 2019. Numerical modeling and dynamic response of 160,000-m^3 liquefied natural gas outer tank under aircraft impact. *Journal of Performance of Constructed Facilities*, 33(4):04019039. https://doi.org/10.1061/(ASCE)CF.1943-5509.0001307

Zhang RF, Weng DG, Ren XS, 2011. Seismic analysis of a LNG storage tank isolated by a multiple friction pendulum system. *Earthquake Engineering and Engineering Vibration*, 10(2):253-262. https://doi.org/10.1007/s11803-011-0063-3

Zhang T, Wu H, Fang Q, et al., 2017. UHP-SFRC panels subjected to aircraft engine impact: experiment and numerical simulation. *International Journal of Impact Engineering*, 109:276-292. https://doi.org/10.1016/j.ijimpeng.2017.07.012

Zhang T, Wu H, Huang T, et al., 2018. Penetration depth of RC panels subjected to the impact of aircraft engine missiles. *Nuclear Engineering and Design*, 335:44-53. https://doi.org/10.1016/j.nucengdes.2018.04.025

中文概要

题　目： 大型液化天然气储罐在冲击荷载下的动力响应数值研究

目　的： 研究冲击荷载各参数对于液化天然气（LNG）储罐的动力响应结果，定义 LNG 储罐受到冲击荷载时的破坏模式，并分析不同破坏模式下的破坏机理，为工程防御冲击荷载提供有效的理论研究基础。

创新点： 1. 建立精细化的 LNG 储罐有限元模型；2. 定义 LNG 储罐在冲击荷载下的破坏模式并揭示其破坏机理；3. 提出损伤因子 D_f 可区分三种冲击破坏模式。

方　法： 1. 通过有限元模拟，进行冲击荷载的参数分析，得到不同冲击荷载对于 LNG 储罐的动力响应（图 6 和 7）；2. 根据数值模拟结果，定义 LNG 储罐受到冲击荷载时的破坏模式（图 8），并分析其破坏机理（图 10 和 11）；3. 通过经验公式验算 LNG 储罐抵御冲击荷载的可靠性。

结　论： 1. LNG 储罐薄弱部位为外罐和环梁及底板的连接部位；2. LNG 储罐受到冲击荷载的破坏模式分为局部变形、混凝土剥落和穿透三种；本研究得到了各种破坏模式下的破坏机理，并定义了损伤因子 D_f 来区分三种破坏模式；3. 通过经验公式验算，LNG 储罐可以抵御英国规范建议的冲击荷载和法兰的冲击；DOE-standard 公式计算结果最为保守。

关键词： LNG 储罐；冲击；动力响应；数值模拟；破坏机理